Research Article

Baboucarr Ceesay, Muhammad Z. Baber, Nauman Ahmed, Naveed Shahid, Siegfried Macías, and Jorge E. Macías-Díaz*

Abundant wave symmetries in the (3+1)-dimensional Chafee–Infante equation through the Hirota bilinear transformation technique

https://doi.org/10.1515/phys-2025-0176
received February 25, 2025; accepted May 23, 2025

Abstract: The present study investigates different types of wave symmetries in the (3 + 1)-dimensional Chafee–Infante equation *via* the Hirota bilinear transformation technique. In this work, we derived exact solutions that include bright and dark solitons, periodic cross kink, multiple waves, mixed waves, homoclinic breathers, M-shaped related waves and periodic lump waves. These solutions exhibit stability, energy confinement, and dynamic interactions. It is observed that the Hirota method captures the highly nonlinear complex phenomena that result from the balance between the nonlinearity and the dispersion. These factors lead to a stability and coherent formation of wave forms. We employed Mathematica 11.1 software to obtain 3D, contour, and 2D graphs of our solution. The graphs present the spatial and temporal evolution of these solutions. The periodic structures, oscillatory solitons, and cross-kink configurations have dynamic interaction while maintaining fundamental properties of waves. Breather and homoclinic breather solutions present the basis of oscillatory local dynamics, which stress on energy transfer and phase modulation. The novelty of this article is in the use of the Hirota bilinear technique to the Chafee–Infante equation in (3 + 1)-dimensional dimension, which allows the derivation of a wide variety of exact multidimensional wave solutions, including intricate hybrid solutions previously unreported for the equation. This provides great value by extending the analytical theory and improving the understanding of nonlinear wave behaviors in high-dimensional environments. It is worth noting that all the solutions have been verified and found to satisfy the governing equation.

Keywords: (3+1)-dimensional Chafee–Infante equation, Hirota bilinear method, soliton solutions, M-shaped waves, breather waves, lump solutions, rogue waves, kink and anti-kink structures, wave interaction, nonlinear wave dynamics, multidimensional solitons, periodic cross-kinks, exact analytical solutions

*** Corresponding author: Jorge E. Macías-Díaz,** Department of Mathematics and Physics, Autonomous University of Aguascalientes, Aguascalientes, Mexico; Department of Mathematics and Didactics of Mathematics, Tallinn University, Tallinn, Estonia,
e-mail: jorge.maciasdiaz@edu.uaa.mx, jemacias@correo.uaa.mx
Baboucarr Ceesay: Department of Mathematics and Statistics, The University of Lahore, Lahore, Pakistan; Mathematics Unit, The University of The Gambia, Kanifing, The Gambia
Muhammad Z. Baber: Department of Mathematics and Statistics, The University of Lahore, Sargodha Campus, Sargodha, Pakistan
Nauman Ahmed, **Naveed Shahid:** Department of Mathematics and Statistics, The University of Lahore, Lahore, Pakistan
Siegfried Macías: Department of Mathematics and Physics, Autonomous University of Aguascalientes, Aguascalientes, Mexico

1 Introduction

Solitons are solitary waves (or self-reinforcing waveforms) that travel at a constant speed, keeping their shape in the way. They form the core of nonlinear science, and they result from the balance of nonlinearity and dispersion. As a consequence, they are critical to understanding several fundamental physical and mathematical systems. Solitons abound in most fields, such as fluid [1], plasma physics [2], optical communication [3], stellar environments [4], and biology [5], to mention only a few. Among many equations modeling the behavior of solitons, such as the nonlinear chains of atoms model [6], the bistable Allen-Cahn equation [7], and the coupled nonlinear Schrüdinger-type equations [8], as well as the (3 + 1)-dimensional Calogero–Bogoyavlenskii–Schiff (CBS) equation, the CBS–Bogoyavlensky–Konopelchenko (CBS-BK) equation [9], the unstable NLSE and the modify unstable NLSE [10], and so on, the Chafee–Infante equation (CIE) can rightly be classified as a celebrated reaction–diffusion model [11]. This equation describes the energy balance between equator and pole of the solar system, which transmit energy *via* heat diffusion [12].

The one-dimensional CIE has emerged as one important topic of mathematical research. This equation has been analyzed with the sole aim of discovering its attractor structure and developing various stability characteristics [13]. For example, Caraballo *et al.* [14] shed light on the effects of stochastic perturbations on this equation through their investigations, which led to an intriguing conclusion on the noise and system synthesis. Such investigations showed how multiplicative Itô noise could stabilize the origin, while Stratonovich noise preserved the attractor's dimension. They also showed that sufficiently rich additive noise could reduce the random attractor to a single point. They also emphasized the importance of noise in modulating the dynamics of reaction–diffusion systems. In turn, Debussche *et al.* [15] addressed thoroughly the deterministic CIE with special reference to its long-time dynamics and attractor structures. Their work showed how stable and unstable manifolds direct solutions toward equilibrium. The initial results formed a basis for future research efforts concerning the equation's response to perturbations and modification of parameters.

Undoubtedly, the CIE has been extended from the one-dimensional case into higher-dimensional transitions. An application of the equation to mass transport, particle diffusion, and energy transfer has been made for two and three spatial dimensions. Rosa [16] applied the inertial manifold theory in designing exact finite-dimensional feedback control laws for the equation to demonstrate its potential in control theory. The investigation highlighted the capacity of the CIE as a model for the controlled nonlinear systems. As a follow-up, Carvalho *et al.* [17] studied the nonautonomous version of the equation, providing a detailed analysis of its pullback attractor structure and the bifurcations that arise when parameters are varied. Such works are examples of dynamic behavior captured with this versatile equation in various settings. In addition, stochastic modifications of the CIE have also attracted much interest. Blumenthal [18] investigated pitchfork bifurcations in the face of stochastics and found that, even with the destruction of random pullbacks, finite-time Lyapunov exponents persist. The contribution provides new prospects the regarding bifurcation theory in stochastic systems by demonstrating that noise acts to simultaneously destabilize and preserve important dynamical features.

On the other hand, analytical techniques have played a very vital role in exploring the solutions and properties of the CIE. For example, using the modified F-expansion method, Tang and Wang [19] derive bright and kink soliton solutions and provide stability analyses of their behavior. Hossain *et al.* [20] have contributed to this work by incorporating conformable fractional derivatives into this equation and discovering multisoliton interactions and waveforms in trigonometric, hyperbolic, and exponential forms by applying the nonlinear M-shaped expansion method. More work has been done concerning novel solutions of the CIE. Rached [21] used the enhanced modified simple equation method to construct exact solutions and extend the range of analytical solutions known until now. Mahmood *et al.* [22] presented the modified Khater method for solving the (2+1)-dimensional version of the equation that describes a wide variety of propagating wave patterns, including bright and dark solitons, as well as periodic solitons. Arshed *et al.* [23] employed this equation to gain soliton solutions in hyperbolic, trigonometric, and rational form with the extended $\frac{G'}{G^2}$-expansion method and new $\frac{F}{G}$-expansion method. The applicability of the equation was further highlighted for phenomena in fluid-dynamics, plasma physics, and nonlinear optical systems. They stressed the role of conservation laws in understanding the integrability of the equation.

Furthermore, Arshed *et al.* [24] hastened the study of this equation by finding solutions such as bright, dark, periodic, kink, anti-kink, and singular traveling wave patterns with the extended sinh-Gordon equation expansion technique. Kumar *et al.* [25] employed the generalized exponential rational function (GERF) technique to derive quite a number of soliton solutions to the (2+1)-dimensional CIE. Their work yielded closed-form solutions in the form of bright soliton and dark solitons, combined and singular profiles, periodic oscillatory waves, and kink-wave structures. Akbar *et al.* [26] used first integral method to realize solitary wave solution for NLEEs such as CIE. They showed how the solutions obtained can be used in physical applications. Also, Cimpoiasu [27] put forth an introduction of a modified auxiliary equation (MAE) method associated with stochastic differential equations for soliton solution investigation of the CIE. This new method uses stochastic processes such as Wiener process to study magnitude and behavior of solitons under their stochastic influences. Their work brought in new insights into the stochastic dynamics of solitons and helps for understanding soliton behavior against random perturbations. Khater and Ghanbari [28] also employed the generalized expansion method to solve this equation under time-variable coefficients. Such an approach included nonlinear wave variables along with auxiliary equations such as Riccati equations and Jacobian elliptic equations to present nonautonomous solutions formed by triangular, rational, or doubly-periodic structures showing the effect of variable coefficients on the performance of solitons.

It is worth noting that the studies mentioned earlier were all based on either (1 + 1) or (2 + 1)-dimensions. From the literature, one of the few works on the

(3 + 1)-dimensional CIE are those by Sebogodi *et al.* [29], who derived soliton solutions using methods such as GERF, first integral, and expansion techniques. Likewise, Khater and Alfalq [30] employed the fractional nonlinear generalized (3 + 1)-dimensional CIE to model wave propagation in dispersive media. However, these include analytical and numerical solutions that demonstrate that wave dynamics were simulated efficiently using the Khat II and He's variational iteration method. Collectively, these works speak of the multifunctional character of the equation as a model of nonlinear systems. The results embody the efforts to create and sustain high-level computations for the interpretation of analytical solutions. The generalized (3+1)-dimensional CIE provides an important ground to harvest nonlinear wave dynamics in multidimensional systems. This equation is formulated in the form [29]

$$N_{xt} - N_{xxx} + aN^3N_x + bN_x + cN_{yy} + dN_{zz} = 0, \qquad (1)$$

where $N(x, y, z, t)$ represents the wave function in the entering parameters a, b, c, and d, which govern the nonlinearity and dispersion as well as the reaction–diffusion effects. Also, higher dimensional terms make this equation a candidate for very complex interactions, like in the case of high energy physical processes, environmental systems, or optical waveguides. The model is an essential generalization of the reaction–diffusion model, where extra spatial directions are added to explain intricate wave behavior in systems of higher dimension. The model has important implications in nonlinear optics for explaining propagation of ultrashort pulses through multimode fibers, in plasma physics for understanding ion-acoustic waves in magnetized plasmas, and in fluid mechanics for studying formation of rogue waves in three-dimensional oceanic domains. The inclusion of multiple spatial dimensions (y, z) enables cross-directional wave interaction and pattern formation to be examined, making it especially applicable for the understanding of energy transport in anisotropic media. In the quantum field theory, it can be used as a model for the investigation of spontaneous symmetry breaking in (3 + 1)-dimensional systems. The nonlinear terms of the model account for key aspects of wave self-focusing and modulation instability, while its dispersive terms explain wave broadening effects, making it important in predicting extreme wave events in natural and engineered systems. Recent uses include biophysics to model signal propagation in three-dimensional neural networks and materials science to analyze nonlinear elastic waves in crystalline materials. The versatility of the equation to accommodate various solution types (solitons, breathers, rogue waves) under various parameter regimes renders it a valuable instrument for exploring nonlinear wave phenomena across various disciplines.

The Hirota bilinear transformation technique has proven to be a very capable device both for the solving of nonlinear partial differential equations and the discovery of different forms of wave phenomena, such as solitons, breathers, lumps, M-shaped, periodic, kink, and rogue waves. By demonstrating the versatility of this technique, Yin *et al.* [31] took this procedure into (3 + 1)-dimensional equations to facilitate rational transformations for deriving complex solutions of generalized shallow water wave equations that present rogue waves and interaction solutions. Furthermore, Li *et al.* [32] proposed an extended Hirota's method developing modification rules in summation to reveal more complicated structures as M-shaped, molecular, or web-like solitons in the (2+1) Sawada-Kotera equation and much more. These improvements highlight the flexibility of the method to give suitable treatment for complex wave motions within a variety of dimensions and contexts. More researchers delve into real-life application and computational techniques for Hirota's method. However Yokus and Isah [33] go a step further and combine it with a new exponential function technique to study sections of KdV solutions about soliton stability and nonlinear wave interaction. Zhang *et al.* [34] considered shock wave responses of equations of type KdV–Burgers and Zakharov–Kuznetsov–Burgers and tried to relate them to dissipation effects with physical wave behavior. According to Ceesay *et al.* [35] about M-soliton solutions of the modified regularized long wave equation, these reflect real life in terms of coastal dynamics with possible insights into sediment transport and erosion effects. Kumar and Mohan [36] on the hand gain multi-soliton solutions to high-dimensional equations using this method. Ahmad *et al.* [37] applied to nonlocal KdV equations and came out with bright soliton solutions with some interesting features. By using the Hirota bilinear transformation technique, Gu *et al.* [38] analyzed the (2+1)-dimensional Kadomtsev–Petviashvili–Sawada–Kotera–Ramani (KPSKR) equation, obtaining its soliton, breather, and lump solutions, and explore their interactions along with the concerned chaotic dynamics of the model. In a similar work, Gu *et al.* [39] also explore the (3+1)-dimensional Kadomtsev–Petviashvili–Boussinesq-like equation employing the same approach to derive soliton, lump, and traveling wave solutions as well as exploring the model's chaotic behavior. Shehzad *et al.* [40] used the Hirota bilinear method for a wider set of nonlinear wave structures such as lump, rogue, breather, and periodic waves, with focus on their interactions and physical importance in plasma systems, ocean wave dynamics, and other realistic applications. These works and numerous others prove the profound effect that the Hirota bilinear method has on mathematical

physics, applied sciences, and the changing of theoretical insights into the practical domain.

Despite significant advances in studying the CIE in lower dimensions, not much work has been done investigating its (3+1)-dimensional version using the Hirota bilinear transformation method. This research fills that void by deriving a wide range of exact wave solutions such as bright and dark solitons, breathers, lumps, M-shaped waves, and periodic cross kink waves within this higher dimensional context. The novelty of this work lies in the rigorous application of Hirota's technique for deriving and visualizing intricate wave interactions that are still analytically manageable but dynamically complex. These results not only deepen the theory of soliton dynamics in multidimensional systems but also expand the applicability of the CIE to nonlinear waves in physics and engineering. Hence, this work enhances the study of nonlinear wave analysis and provides a solid base for further theoretical research and applications in real-life situations concerning multidimensional soliton phenomena.

The rest of this article is structured as follows. In Section 2, the Hirota bilinear approach is briefly reviewed, and the bilinear form of the (3+1)-dimensional CIE is established. We also exhibits a set of exact solutions for this model. In Section 3, we highlight the graphical representations and a detailed analysis of the dynamical behavior of these solutions. Section 4 shows the results comparison of the manuscript, and Section 5 ends the article by summarizing main findings and possible areas of the future work.

2 The Hirota bilinear method

The Hirota bilinear technique is a popular and powerful analytical method for determining exact solutions of nonlinear partial differential equations (NLPDEs). Its main advantage consists of being systematic and constructive in nature, enabling to derive soliton, lump, breather, and other interactive solutions without needing to linearize or approximate. The technique operates effectively by transforming the NLPDE into a bilinear form through dependent variable transformations so that the process of solution can be treated algebraically. Another benefit is that it can treat multisoliton and higher-dimensional solutions, and it is appropriate for the investigation of complex wave structures such as those in the (3+1)-dimensional CIE examined in this research. In addition, it allows one to build up solutions with controllable parameters for in-depth wave behavior, stability, and interactions analysis.

There are, however, some weaknesses in the approach. One is that it commonly depends on specific transformations and assumptions (e.g., exponential forms of the solutions), which are not necessary for all forms of nonlinear equations especially nonpolynomial or nonintegrable ones. Also, the approach does not deal with boundary or initial conditions directly, so its use is mainly within the framework of determining formal exact solutions but not complete boundary value problems. Moreover, although the bilinear form is compact, the algebra may grow more complicated when dealing with higher-order or generalized equations, necessitating the use of symbolic computation tools for effective application. In spite of these constraints, the Hirota method is still a very efficient and flexible method, particularly for researchers who wish to investigate the rich structure of nonlinear wave dynamics in both lower and higher dimensions.

We now proceed to use this method in Eq. (1). To do so, first, we make the Cole–Hopf transformation; that is, we take the logarithmic transformation of the dependent variable N, giving us the assumption that the solution to Eq. (1) is,

$$N(x, y, z, t) = R(\ln(k(x, y, z, t)))_x, \tag{2}$$

where R is a constant to be determine. To find R, we begin by using the following function:

$$N(x, y, z, t) = e^{\alpha_i x + \beta_i y + \lambda_i z} + \omega_i t, \tag{3}$$

where α_i, β_i, and λ_i represent the wave numbers, and ω_i represents the dispersion. By putting Eq. (3) into the linear parts of Eq. (1), we obtain the dispersion relation as follows:

$$\omega_i = \frac{-b\alpha_i - c\beta_i^2 - d\lambda_i^2 + \alpha_i^3}{\alpha_i}. \tag{4}$$

We now replace the function

$$k(x, y, z, t) = \exp\left(\frac{t(-b\alpha_i - c\beta_i^2 - d\lambda_i^2 + \alpha_i^3)}{\alpha_i} + x\alpha_i + y\beta_i + z\lambda_i\right) + 1, \tag{5}$$

into the Cole–Hopf transformation in Eq. (2), and by using the result in Eq. (1), we can solve for R to obtain

$$R = \frac{\sqrt{6}}{\sqrt{a}}. \tag{6}$$

Therefore, the logarithmic transformation becomes

$$N = \frac{\sqrt{6}}{\sqrt{a}}(\ln(k(x, y, z, t)))_x. \tag{7}$$

We transformed the linear terms of Eq. (1) into bilinear form as follows:

$$k\frac{\partial^2 k}{\partial x\partial t} + bk\frac{\partial k}{\partial x} + ck\frac{\partial^2 k}{\partial y^2} - c\left(\frac{\partial k}{\partial y}\right)^2 + dk\frac{\partial^2 k}{\partial z^2} - d\left(\frac{\partial k}{\partial z}\right)^2 - k\frac{\partial^3 k}{\partial x^3} + 3\frac{\partial k}{\partial x}\frac{\partial^2 k}{\partial x^2} - \frac{\partial k}{\partial x}\frac{\partial k}{\partial t} = 0. \tag{8}$$

We would enter into Eq. (8) all forms of wave functions under study with means of Mathematica. Then for each specific case, we will expand and evaluate and arrange related terms as related to one another, setting them to 0. This will lead us to solutions of these systems of equations, finding various potential families corresponding to each case.

(1) **Interaction *via* double exponents:** This wave structure is given in the following equation [41]:

$$k(x,y,z,t) = P_1\exp(h(L_1(tw + x + y + z) + L_2)) + P_2\exp(h(L_3(tw + x + y + z) + L_4)). \tag{9}$$

When Eq. (9) and its first three partial derivatives are substituted into Eq. (8), and the resulting expression simplified, the like terms are combined, and the coefficients of each term are set equal to zero, we obtain the following categories of constant values.

Category 1: $L_1 = 0, L_3 = -\frac{i\sqrt{b}}{\sqrt{2}h}, w = -\frac{3i\sqrt{b}}{\sqrt{2}} - c - d$. If we put them into Eq. (9) and inject the outcome into Eq. (7), we obtain the result as follows:

$$N_{1IE}(x,y,z,t) = -\frac{i\sqrt{3}\sqrt{b}P_2 e^{hL_4 + \frac{i\sqrt{b}(ct+dt-x-y-z)}{\sqrt{2}}}}{\sqrt{a}\left(P_1 e^{\frac{3bt}{2}+hL_2} + P_2 e^{hL_4 + \frac{i\sqrt{b}(ct+dt-x-y-z)}{\sqrt{2}}}\right)}. \tag{10}$$

Category 2: $L_1 = \frac{i\sqrt{b}}{\sqrt{2}h}$, $L_3 = -\frac{i\sqrt{b}}{\sqrt{2}h}$, $w = -c - d$. If we put them into Eq. (9) and inject the outcome into Eq. (7), we obtain the result as follows:

$$N_{2IE}(x,y,z,t) = \frac{i\sqrt{3}\sqrt{b}(-P_2 e^{hL_4} + P_1 e^{hL_2 + i\sqrt{2}\sqrt{b}(-ct-dt+x+y+z)})}{\sqrt{a}(P_2 e^{hL_4} + P_1 e^{hL_2 + i\sqrt{2}\sqrt{b}(-ct-dt+x+y+z)})}. \tag{11}$$

(2) **Interaction of M-shaped rational wave with one kink:** This wave configuration is provided in the following equation [41]:

$$k(x,y,z,t) = P_1\exp(L_1(tw + x + y + z) + L_2) + (L_3(tw + x + y + z) + L_4)^2 + (L_5(tw + x + y + z) + L_6)^2 + L_7. \tag{12}$$

The following category of constant value is obtained when Eq. (12) and its first three partial derivatives are substituted into Eq. (8) and the resulting expression simplified. The like terms in the expression combined and the coefficients of each term set to zero.

Category 1: $L_1 = -\frac{i\sqrt{b}}{\sqrt{2}}, L_3 = 0, L_5 = 0, w = -\frac{3i\sqrt{b}}{\sqrt{2}} - c - d$. By substituting them into Eq. (12) and then substituting the result into Eq. (7), we obtain

(3) **Interaction of M-shaped rational wave with rogue and kink:** This wave configuration is provided in the following equation [41]:

$$N_{1M1K}(x,y,z,t) = \frac{12L_1(w_4^2 + w_6^2 + w_7)(m^2 - u_0^2(u_2+1))\exp\left(\frac{\sqrt{m^2 - u_0^2(u_2+1)}(mt+x)}{m\sqrt{u_1}} + w_2\right)}{m^2\left(L_1 e^{w_2} + (w_4^2 + w_6^2 + w_7)e^{\frac{\sqrt{m^2-u_0^2(u_2+1)}(mt+x)}{m\sqrt{u_1}}}\right)^2}. \tag{13}$$

$$k(x,y,z,t) = P_2\exp(L_3(tw + x + y + z) + L_4) + P_1\cosh(L_1(tw + x + y + z) + L_2) + (L_5(tw + x + y + z) + L_6)^2 + (L_7(tw + x + y + z) + L_8)^2 + L_9. \tag{14}$$

Eq. (14) and its partial derivatives up to third order are substituted into Eq. (8), followed by simplification. The like terms are then collected so that for every expression, the coefficients of each expression set to zero. Thus, a category of constant values emerges from this system of equations:

Category 1: $L_1 = -\frac{i\sqrt{b}}{\sqrt{2}}$, $L_3 = -\frac{i\sqrt{b}}{\sqrt{2}}$, $L_5 = -iL_7$, $L_6 = 0$, $L_8 = 0$, $L_9 = 0$, $w = -c - d$. When we substitute these into Eq. (14) and insert the outcome into Eq. (7), we then end up with the result as follows:

$$N_{1MRK}(x,y,z,t) = -\frac{\sqrt{3}\sqrt{b}\left(P_1 e^{\frac{i\sqrt{b}(-ct-dt+x+y+z)}{\sqrt{2}}}\sin\left(\frac{\sqrt{b}(-ct-dt+x+y+z)}{\sqrt{2}} + iL_2\right) + ie^{L_4}P_2\right)}{\sqrt{a}\left(e^{L_4}P_2 + P_1 e^{\frac{i\sqrt{b}(-ct-dt+x+y+z)}{\sqrt{2}}}\cos\left(\frac{\sqrt{b}(-ct-dt+x+y+z)}{\sqrt{2}} + iL_2\right)\right)}. \tag{15}$$

(4) **Mixed waves:** This wave configuration is provided in the following equation [42]:

$$\begin{aligned} k(x,y,z,t) &= P_1\exp(h(L_1(tw+x+y+z)+L_2)) \\ &+ P_2\exp(-h(L_1(tw+x+y+z)+L_2)) \\ &+ P_3\sin(h(L_3(tw+x+y+z)+L_4)) \\ &+ P_4\sinh(h(L_5(tw+x+y+z)+L_6)). \end{aligned} \tag{16}$$

While substituting Eq. (16) along with its three immediate partial derivatives into Eq. (8), a simplified expression emerged. Then we grouped similar terms together, and for every expression, set its coefficient equal to zero. This provides us with the following categories of constant values:

Category 1: $L_1 = -\frac{i\sqrt{b}}{\sqrt{2}h}$, $L_3 = \frac{\sqrt{b}}{\sqrt{2}h}$, $L_5 = -\frac{i\sqrt{b}}{\sqrt{2}h}$, $w = -c - d$. By inserting them into Eq. (16), and then the result into Eq. (7), we have

$$N_{1MI}(x,y,z,t) = \frac{\sqrt{3}\sqrt{b}\left(iP_2e^{i\sqrt{2}\sqrt{b}(t(-(c+d))+x+y+z)} + F_1 + (-i)P_1e^{2hL_2}\right)}{\sqrt{a}\left(P_2e^{i\sqrt{2}\sqrt{b}(t(-(c+d))+x+y+z)} + F_2 + P_1e^{2hL_2}\right)}, \tag{17}$$

where

$$\begin{aligned} F_1 &= \left(P_3\cos\left(\frac{\sqrt{b}(t(-(c+d))+x+y+z)}{\sqrt{2}} + hL_4\right)\right. \\ &\left. - iP_4\cos\left(\frac{\sqrt{b}(t(-(c+d))+x+y+z)}{\sqrt{2}} + ihL_6\right)\right) \\ &\cdot\exp\left(hL_2 + \frac{i\sqrt{b}(t(-(c+d))+x+y+z)}{\sqrt{2}}\right), \\ F_2 &= \left(P_3\sin\left(\frac{\sqrt{b}(t(-(c+d))+x+y+z)}{\sqrt{2}} + hL_4\right)\right. \\ &\left. - iP_4\sin\left(\frac{\sqrt{b}(t(-(c+d))+x+y+z)}{\sqrt{2}} + ihL_6\right)\right) \\ &\cdot\exp\left(hL_2 + \frac{i\sqrt{b}(t(-(c+d))+x+y+z)}{\sqrt{2}}\right). \end{aligned}$$

Category 2: $P_2 = 0$, $L_1 = \frac{i\sqrt{b}}{\sqrt{2}h}$, $L_3 = \frac{\sqrt{b}}{\sqrt{2}h}$, $L_5 = -\frac{i\sqrt{b}}{\sqrt{2}h}$, $w = -c - d$. If we substitute them into Eq. (16) and then that result into Eq. (7), we have

$$N_{2MI}(x,y,z,t) = \frac{i\sqrt{3}\sqrt{b}\left(-F_3 + P_1\exp\left(hL_2 + \frac{i\sqrt{b}(t(-(c+d))+x+y+z)}{\sqrt{2}}\right)\right)}{\sqrt{a}\left(F_4 + P_1\exp\left(hL_2 + \frac{i\sqrt{b}(t(-(c+d))+x+y+z)}{\sqrt{2}}\right)\right)}, \tag{18}$$

where

$$\begin{aligned} F_3 &= iP_3\cos\left(\frac{\sqrt{b}(t(-(c+d))+x+y+z)}{\sqrt{2}} + hL_4\right) \\ &- P_4\cos\left(\frac{\sqrt{b}(t(-(c+d))+x+y+z)}{\sqrt{2}} + ihL_6\right), \\ F_4 &= P_3\sin\left(\frac{\sqrt{b}(t(-(c+d))+x+y+z)}{\sqrt{2}} + hL_4\right) \\ &- iP_4\sin\left(\frac{\sqrt{b}(t(-(c+d))+x+y+z)}{\sqrt{2}} + ihL_6\right). \end{aligned}$$

(5) **Multiwaves:** This pattern of waves is offered in [42]

$$\begin{aligned} k(x,y,z,t) &= P_2\cos(L_3(tw+x+y+z)+L_4) \\ &+ P_1\cosh(L_1(tw+x+y+z)+L_2) \\ &+ P_3\cosh(L_5(tw+x+y+z)+L_6). \end{aligned} \tag{19}$$

By substituting Eq. (19) as well as its first three partial derivatives into Eq. (8) and simplifying the expression, we then group together similar terms and equate them to zero with respect to the coefficient of each expression: The resultant was the following category of constant values:

Category 1: $P_3 = 0, L_1 = \frac{i\sqrt{b}}{\sqrt{2}}, L_3 = \frac{\sqrt{b}}{\sqrt{2}}, w = -c - d$. By plugging them into Eq. (19) and subsequently into Eq. (7), we obtain

$$N_{1MU}(x,y,z,t) = \frac{\sqrt{3}\sqrt{b}\left(P_2\sin\left(\frac{\sqrt{b}(-ct-dt+x+y+z)}{\sqrt{2}} + L_4\right) + P_1\sin\left(\frac{\sqrt{b}(-ct-dt+x+y+z)}{\sqrt{2}} - iL_2\right)\right)}{\sqrt{a}\left(P_2\cos\left(\frac{\sqrt{b}(-ct-dt+x+y+z)}{\sqrt{2}} + L_4\right) + P_1\cos\left(\frac{\sqrt{b}(-ct-dt+x+y+z)}{\sqrt{2}} - iL_2\right)\right)}. \tag{20}$$

(6) **Periodic lump:** This wave structure is given in the following equation [43]:

$$\begin{aligned} k(x,y,z,t) &= (L_1(tw+x+y+z)+L_2)^2 \\ &+ (L_3(tw+x+y+z)+L_4)^2 \\ &+ \cos(L_5(tw+x+y+z)+L_6) + L_7. \end{aligned} \tag{21}$$

By substituting Eq. (21) and its first three partial derivatives into Eq. (8) and simplifying the resulting expression, we will assemble like terms together, and equate each expression's coefficients to zero. We obtained the following category of constant values:

Category 1: $L_1 = iL_3$, $L_2 = 0$, $L_4 = 0$, $L_5 = \frac{\sqrt{b}}{\sqrt{2}}$, $L_7 = 0$, $w = -c - d$. By placing them into Eq. (21) and the outcome into Eq. (7), we obtain the result as follows:

$$N_{1PL}(x,y,z,t) = -\frac{\sqrt{3}\sqrt{b}\tan\left(\frac{\sqrt{b}(-ct-dt+x+y+z)}{\sqrt{2}}+L_6\right)}{\sqrt{a}}. \quad (22)$$

(7) **Periodic cross kink:** This pattern of waves is offered in the following equation [43]:

$$\begin{aligned} k(x,y,z,t) &= P_1\exp(h(L_3(tw+x+y+z)+L_4)) \\ &+ \exp(h(L_1(tw+x+y+z)+L_2)) \\ &+ P_2\cos(h(L_5(tw+x+y+z)+L_6)) \\ &+ P_3\cosh(h(L_7(tw+x+y+z)+L_8))+L_9. \end{aligned} \quad (23)$$

With the substitution of Eq. (23) and its first three partial derivatives into Eq. (8), we simplified the equation. We then assemble and group together similar terms and equate zeroes to each one's coefficient. Thus, we obtain the following categories of constant values:

Category 1: $L_1 = \frac{i\sqrt{b}}{\sqrt{2}h}, L_3 = \frac{i\sqrt{b}}{\sqrt{2}h}, L_5 = -\frac{\sqrt{b}}{\sqrt{2}h}, L_7 = -\frac{i\sqrt{b}}{\sqrt{2}h}$, $L_9 = 0, w = -c-d$. By replacing these into Eq. (23) and then the result into Eq. (7), we obtain

$$N_{1PCK}(x,y,z,t) = \frac{i\sqrt{3}\sqrt{b}\left(F_5+\exp\left(hL_2+\frac{i\sqrt{b}(t(-(c+d))+x+y+z)}{\sqrt{2}}\right)\right)}{\sqrt{a}\left(F_6+\exp\left(hL_2+\frac{i\sqrt{b}(t(-(c+d))+x+y+z)}{\sqrt{2}}\right)\right)}, \quad (24)$$

where

$$\begin{aligned} F_5 &= i\left(P_2\sin\left(\frac{\sqrt{b}(t(-(c+d))+x+y+z)}{\sqrt{2}}-hL_6\right)\right. \\ &\left. + P_3\sin\left(\frac{\sqrt{b}(t(-(c+d))+x+y+z)}{\sqrt{2}}+ihL_8\right)\right) \\ &+ P_1\exp\left(hL_4+\frac{i\sqrt{b}(t(-(c+d))+x+y+z)}{\sqrt{2}}\right), \\ F_6 &= P_2\cos\left(\frac{\sqrt{b}(t(-(c+d))+x+y+z)}{\sqrt{2}}-hL_6\right) \\ &+ P_3\cos\left(\frac{\sqrt{b}(t(-(c+d))+x+y+z)}{\sqrt{2}}+ihL_8\right) \\ &+ P_1\exp\left(hL_4+\frac{i\sqrt{b}(t(-(c+d))+x+y+z)}{\sqrt{2}}\right). \end{aligned}$$

Category 2: $P_1 = 0, L_1 = -\frac{i\sqrt{b}}{\sqrt{2}h}, L_5 = -\frac{\sqrt{b}}{\sqrt{2}h}, L_7 = -\frac{i\sqrt{b}}{\sqrt{2}h}$, $L_9 = 0, w = -c-d$. By substituting them into Eq. (23) and then the result into Eq. (7), we have

$$N_{2PCK}(x,y,z,t) = -\frac{i\sqrt{3}\sqrt{b}\left(F_7-iP_3\sin\left(\frac{\sqrt{b}(-ct-dt+x+y+z)}{\sqrt{2}}+ihL_8\right)\right)}{\sqrt{a}\left(F_8+P_3\cos\left(\frac{\sqrt{b}(-ct-dt+x+y+z)}{\sqrt{2}}+ihL_8\right)\right)}, \quad (25)$$

where

$$\begin{aligned} F_7 &= e^{hL_2-\frac{i\sqrt{b}(-ct-dt+x+y+z)}{\sqrt{2}}} \\ &- iP_2\sin\left(\frac{\sqrt{b}(-ct-dt+x+y+z)}{\sqrt{2}}-hL_6\right), \\ F_8 &= P_2\cos\left(\frac{\sqrt{b}(-ct-dt+x+y+z)}{\sqrt{2}}-hL_6\right) \\ &+ e^{hL_2-\frac{i\sqrt{b}(-ct-dt+x+y+z)}{\sqrt{2}}}. \end{aligned}$$

(8) **Homoclinic breather:** This form of waves is given in the following equation [44]:

$$\begin{aligned} k(x,y,z,t) &= P_1\exp(h(L_1(tw+x+y+z)+L_2)) \\ &+ P_2\exp(-h(L_3(tw+x+y+z)+L_4)) \\ &+ P_3\cos(h(L_5(tw+x+y+z)+L_6)). \end{aligned} \quad (26)$$

With the substitution of Eq. (26) and its first four partial derivatives into (8), and simplified. We then assemble and group together similar terms and equate zeroes to each one's coefficient. Thus, we obtain the following categories of constant values: **Category 1:** $L_1 = iL_5, L_3 = iL_5, w = -c-d, h = \frac{\sqrt{b}}{\sqrt{2}L_5}$. By inserting these into Eq. (26) and then the result into Eq. (7), we obtain

$$N_{1HB}(x,y,z,t) = \frac{i\sqrt{3}\sqrt{b}\left(-F_9+P_1\exp\left(\frac{\sqrt{b}(-2iL_5(ct+dt-x-y-z)+L_2+L_4)}{\sqrt{2}L_5}\right)\right)}{\sqrt{a}\left(F_{10}+P_1\exp\left(\frac{\sqrt{b}(-2iL_5(ct+dt-x-y-z)+L_2+L_4)}{\sqrt{2}L_5}\right)\right)}, \quad (27)$$

where

$$\begin{aligned} F_9 &= P_2 + iP_3\exp\left(\frac{\sqrt{b}(L_4+iL_5(-ct-dt+x+y+z))}{\sqrt{2}L_5}\right) \\ &\times \sin\left(\frac{\sqrt{b}(L_5(-ct-dt+x+y+z)+L_6)}{\sqrt{2}L_5}\right), \\ F_{10} &= P_2 + P_3\exp\left(\frac{\sqrt{b}(L_4+iL_5(-ct-dt+x+y+z))}{\sqrt{2}L_5}\right) \\ &\times \cos\left(\frac{\sqrt{b}(L_5(-ct-dt+x+y+z)+L_6)}{\sqrt{2}L_5}\right). \end{aligned}$$

Category 2: $P_1 = 0, L_3 = -iL_5, w = -c-d, h = \frac{\sqrt{b}}{\sqrt{2}L_5}$. By exporting them into Eq. (26) and then the result into Eq. (7), we have

$$N_{2HB}(x,y,z,t) = \frac{i\sqrt{3}\sqrt{b}\left(P_2 + iP_3 \exp\left(\frac{\sqrt{b}(L_4 - iL_5(-ct - dt + x + y + z))}{\sqrt{2}L_5}\right)\sin\left(\frac{\sqrt{b}(L_5(-ct - dt + x + y + z) + L_6)}{\sqrt{2}L_5}\right)\right)}{\sqrt{a}\left(P_2 + P_3 \exp\left(\frac{\sqrt{b}(L_4 - iL_5(-ct - dt + x + y + z))}{\sqrt{2}L_5}\right)\cos\left(\frac{\sqrt{b}(L_5(-ct - dt + x + y + z) + L_6)}{\sqrt{2}L_5}\right)\right)}. \tag{28}$$

3 Discussion

The 3D figures, their corresponding contours, and 2D plots for the obtained solutions are constructed using Mathematica and are displayed in Figures 1–12, which aid in the visualization of the solutions' characteristics. The 3D surface plot in Figure 1(a) describes the event from the superposition of two exponentially propagating waves that yield a bright solitons, localized wave packets that keep their amplitude and shape while propagating along a certain medium. These solitons are formed as a balance of nonlinearity and dispersion in a single energetic and stable compact form, which is a property common for solitons in nonlinear systems such as shallow water waves and plasmas. The contour plot in Figure 1(b) shows how the soliton's space changes as time progresses. This set of contours is able to visualize the translation of the wave along the x-axis at fixed amplitudes. In Figure 1(c), the 2D plot depicts the amplitude of the solitary wave at $t = 0$ (in red), $t = 1$ (in blue), and $t = 2$ (in green). This indicates that the solitary wave propagates without dispersion, an important feature of soliton dynamics. The 3D graph shown in Figure 2(a) describes wave interactions from two exponential functions demonstrating the interaction of two solitons as they coalescence and then again repulse each other with time, and represents dark solitons which are trough-like structures found within the wave profile. The significant property of soliton dynamics indicates that the solitons have an elastic collision, preserving the shape and velocity. The interaction itself shows the system's nonlinearity and stability. The contour plot in Figure 2(b) shows dark soliton stability in space and time. The oscillating regions of high and low energy density indicate stable wave profiles with dark troughs retaining their positions. In Figure 2(c), the coexistence of dark solitons is depicted in the 2D plots – they are at different moments, with depth and all shapes remaining constant at $t = 0$ (red), $t = 1$ (blue), and $t = 2$ (green), showing a strong robustness and stable dynamics as well as showing how the amplitudes and structures are preserved after the collision. Profiles verify that the interaction is elastic, and no energy is lost during the process.

Figure 3(a) deals with a 3D plot obtained from an M-shaped wave interaction with single kink. It reveals a pronounced M-shaped wave with solely one side being kinked, with the M-shape propagating along the space domain over the time. The kink is a site-specific and abrupt transition in the amplitude of the wave, which may be associated with a nonlinear phenomenon. Such a wave is a traveling wave that bears localized perturbations that, in course of time, do not change their configuration. Figure 3(b) is a contour map showing the M-like structure propagating periodically along with the kink as a sudden and time-consistent discontinuity in phase across space and time. This implies that the system is dynamically stable living under a balance of dispersion and nonlinearity characteristics typical of, for instance, a solitonic wave. The 2D graph in Figure 3(c)

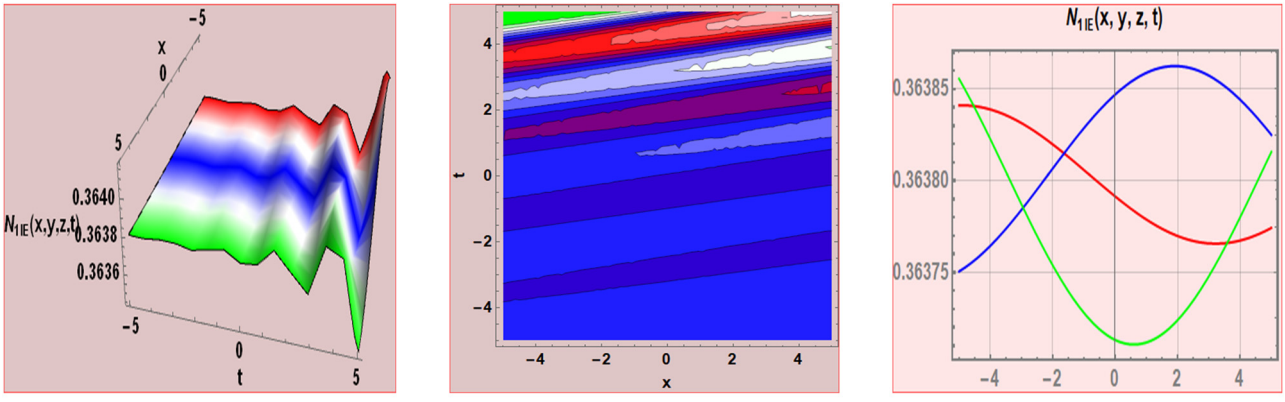

Figure 1: The 3D, contour, and 2D representations depict the interaction through a two-exponent type wave.

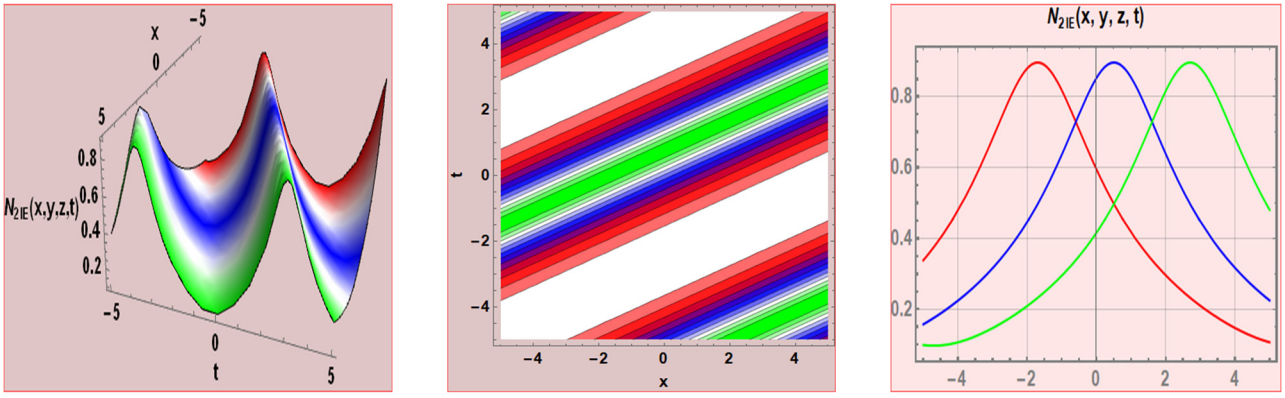

Figure 2: The 3D, contour, and 2D representations depict the interaction through a two-exponent type wave.

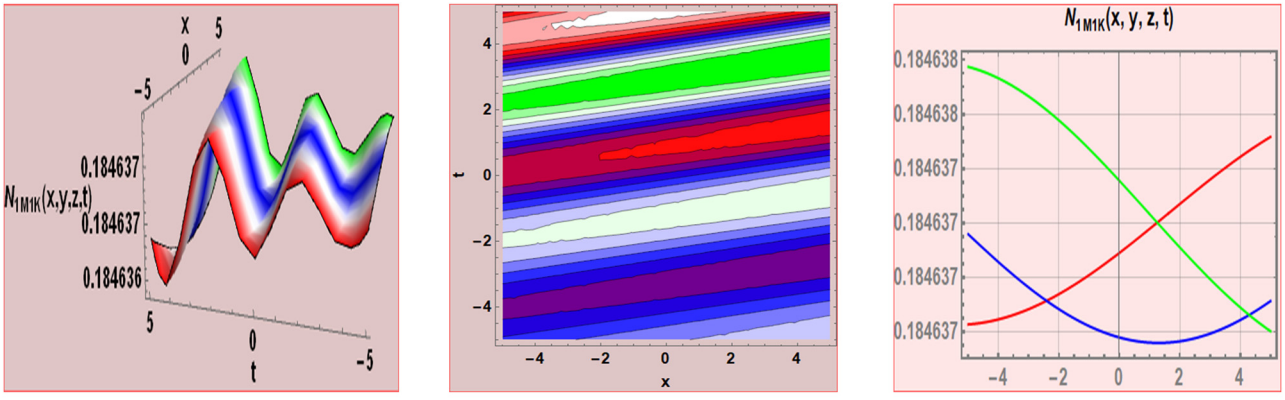

Figure 3: Shows the 3D, contour, and 2D graphs of an M-shaped rational wave containing a single kink.

shows the M-shaped wave profiles at varying time steps ($t = 0$) red, ($t = 1$) blue, and ($t = 2$) green, and how the wave moves while keeping the spatial configuration intact. This is indicative of robustness under propagation, which seems to characterize nonlinear wave systems or traveling wave solutions. Figure 4(a) is a 3D plot showing a wave

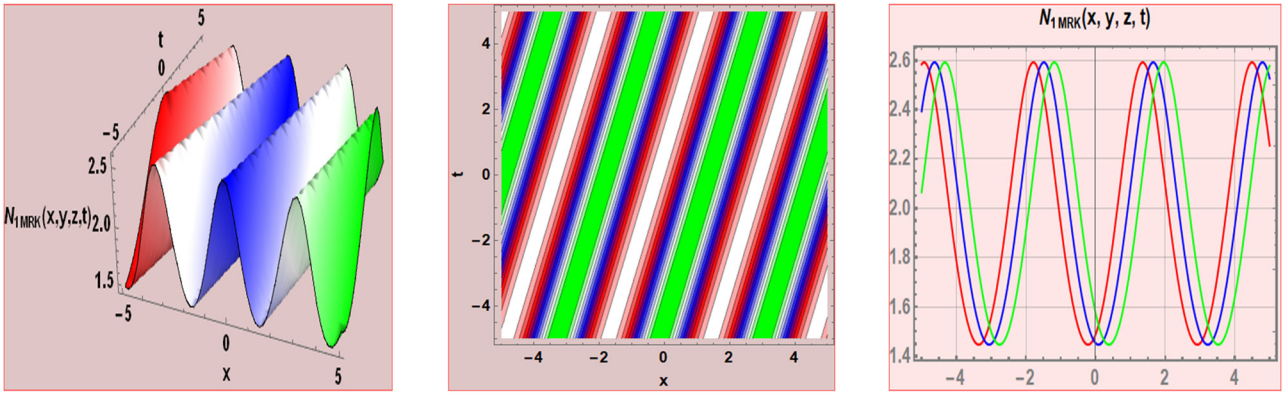

Figure 4: Exhibits a 3D, contour, and 2D charts of an M-shaped rational wave interacting with rogue and kink.

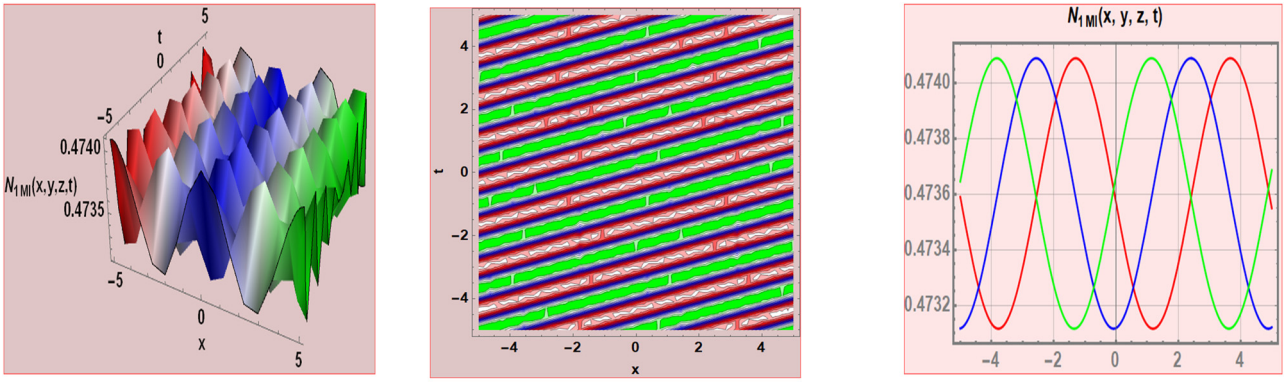

(a) (b) (c)

Figure 5: The 3D, contour, and 2D diagrams are obtained from the mixed waves function.

with an M-shape and acting with rogue and kink. The point of a double peak due to the nonlinear interaction effects. The peaks are symmetric, indicating the equilibrium between effects due to amplitude and dispersion. Figure 4(b) is a contour plot depicting the coherent propagation of M-shaped waves, which exhibit a perfect double-peak structure. An identical geometry of double peaks is thus a sign of their nonlinear stability in time and space. The 2D plots in

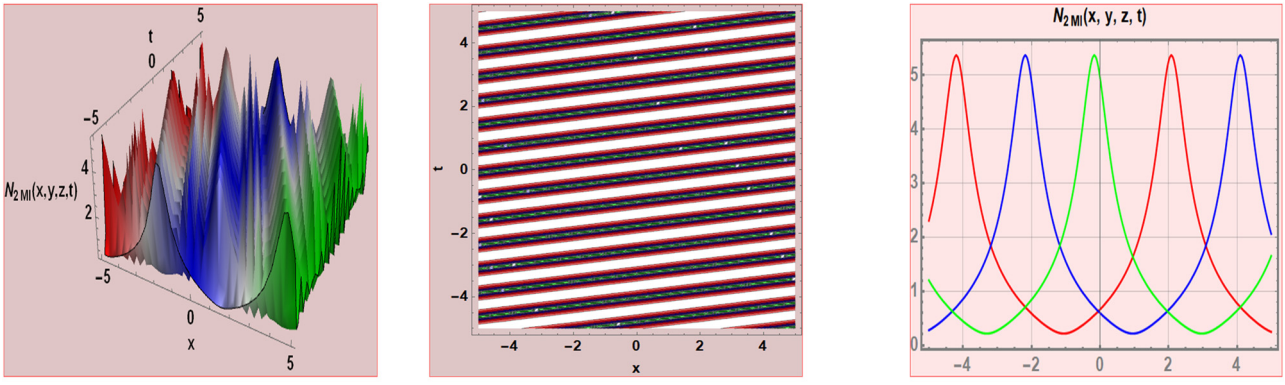

(a) (b) (c)

Figure 6: The 3D, contour, and 2D diagrams are obtained from the mixed waves function.

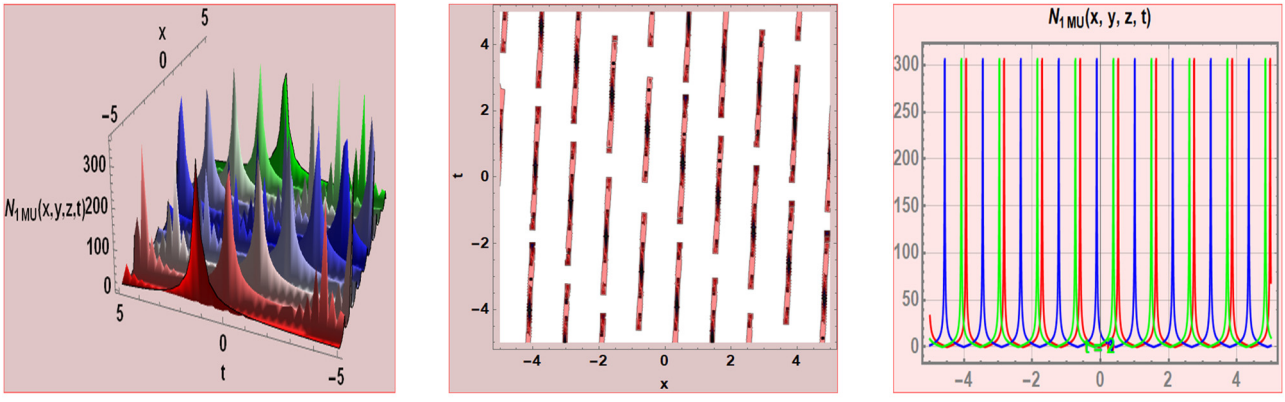

(a) (b) (c)

Figure 7: Displays multiwave types' 3D, contour, and 2D plots.

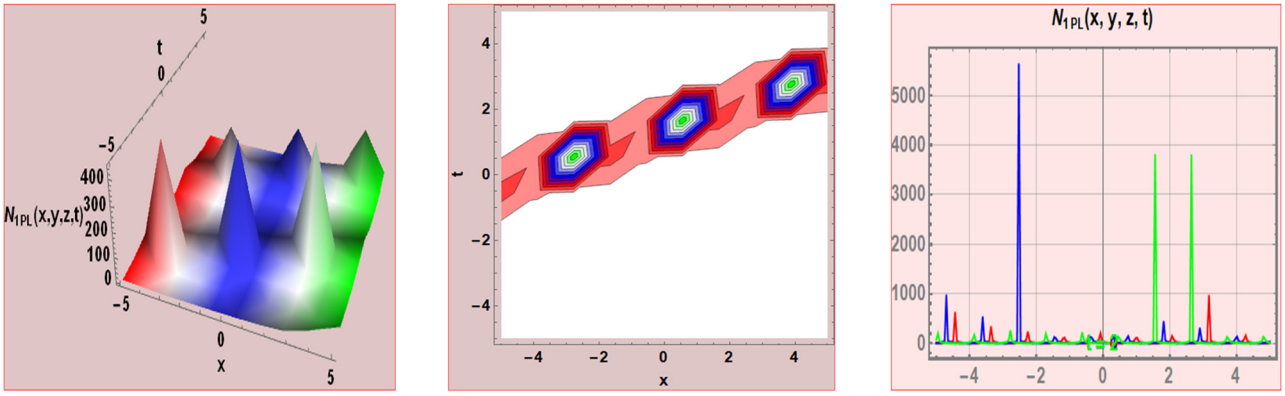

(a) (b) (c)

Figure 8: The 3D, contour, and 2D representations depict the periodic lump-type wave.

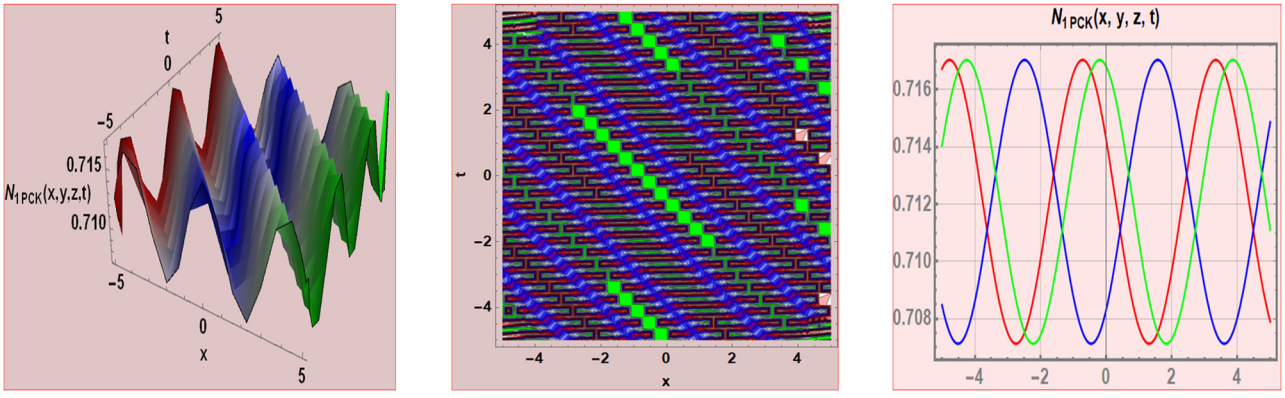

(a) (b) (c)

Figure 9: The 3D, contour, and 2D plots show a periodic cross-kink wave.

Figure 4(c) illustrate the propagation of the M-shaped waves. They have the same symmetrical double peaks, which do not change for $t = 0$ (red), $t = 1$ (blue), and $t = 2$ (green) this confirms its persistence stability.

The 3D illustration in Figure 5(a) is obtained from mixed waves structure. The mixed-frequency wave shows several modes oscillating, thus superimposing the waves as a representation of phenomena like wave interference.

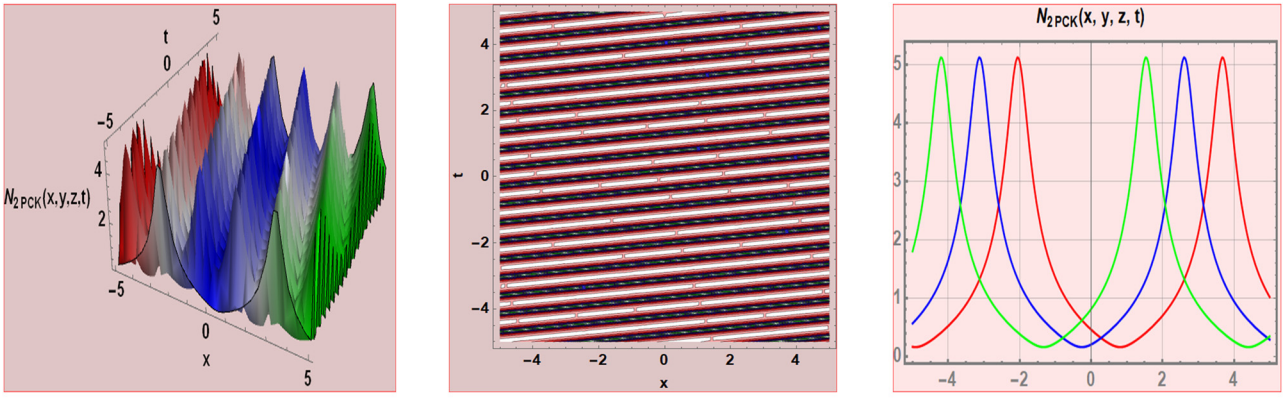

(a) (b) (c)

Figure 10: The 3D, contour, and 2D plots show a periodic cross-kink wave.

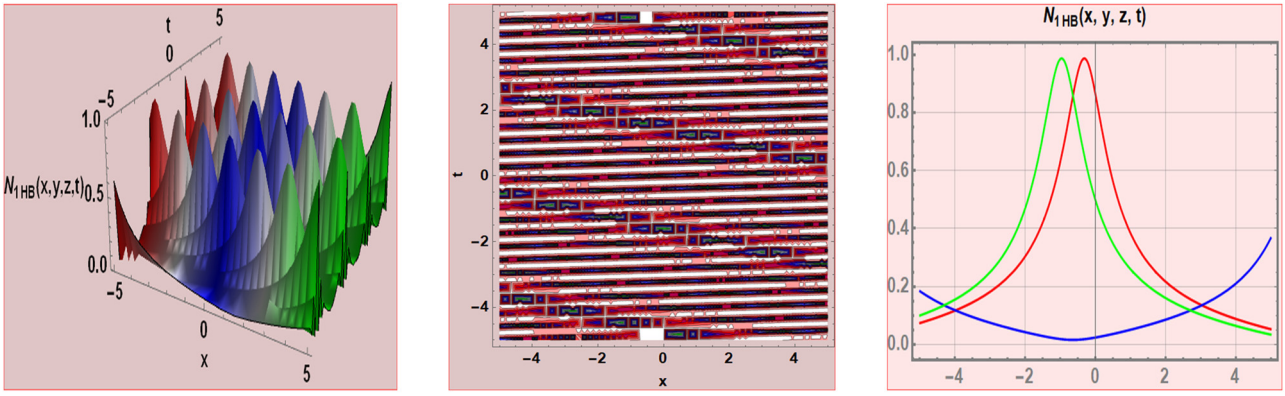

(a) (b) (c)

Figure 11: The homoclinic breather wave is represented *via* 3D, contour, and 2D diagrams.

The contour plot of Figure 5(b) shows the superposed wave forms and in semblance to the structure of a grid, which indicates interaction between different wave frequencies or wavelengths; it may signify constructive and destructive interferences. As indicated in Figure 5(c), the 2D plots of wave amplitude for $t = 0$ (red), $t = 1$ (blue), and $t = 2$ (green). The profiles display the phase and amplitude shifts due to combined effects of waves signifying dynamic interference. The 3D graph of Figure 6(a) is gained from a mixed wave configuration. It shows oscillatory solitons that combine the two features of periodic wave forms as well as localized wave structures in their manifestation. Their motion suggests an equilibrium between the nonlinearity and dispersion, which results in that these repetitive states are always observed to be present even as they oscillate for long periods of time. The contour plot in Figure 6(b) captures the solitons repetitive and oscillatory features whereby the crests of the wave form traces a consistent shape revealing an indication that they propagate through time in a stable fashion with an overall periodic redistribution of energy. The 2D plot in Figure 6(c) indicates representation at $t = 0$ (red), $t = 1$ (blue), and $t = 2$ (green), showing how their movement is oscillatory. The amplitude periodically varies due to the contribution of the effects of focusing and defocusing. Figure 7(a) depicts the 3D plot that shows multi waves interacting. In fact, it show some periodic breather waves. Amplitude oscillation represents the energy exchanged within the system, a phenomenon typical of breather solutions. Figure 7(b) depicts contour plot corresponding to the periodical spatial distribution of the breather waves, confirming the evidence that they form a pattern and grants dynamism with the energy exchange and localization itself. The 2D plot is shown in Figure 7(c) illustrates the oscillatory behavior of the breather waves at $t = 0$ (red), $t = 1$ (blue), and $t = 2$ (green). The stable modulation is what affirms that the breather solution remains so through time.

Figure 8(a) shows a periodic lump wave in a 3D plot that consists of a periodic arrangement of lumps in the

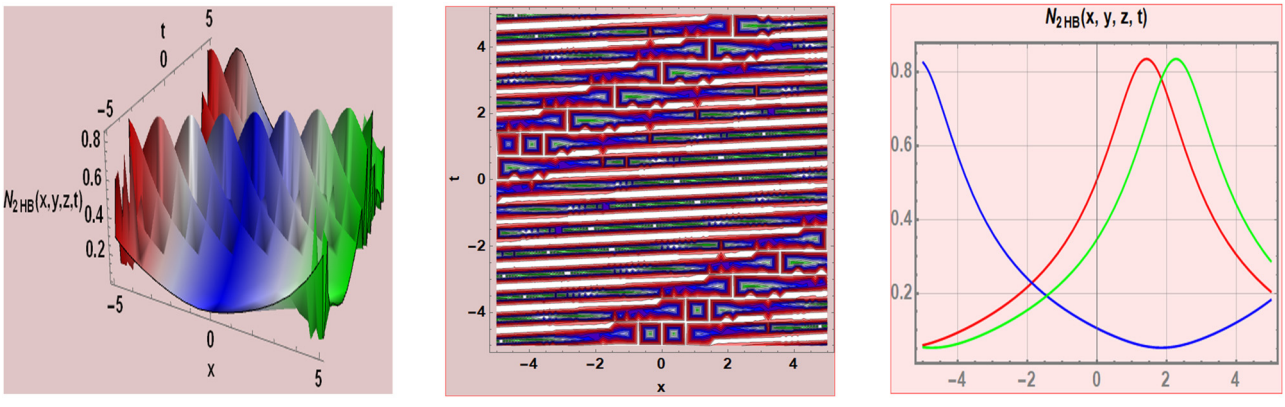

(a) (b) (c)

Figure 12: The homoclinic breather wave is represented *via* 3D, contour, and 2D diagrams.

spatial domain. Each lump exhibits the behavior of a solitary localized wave, similar to a typical lump wave and has an area of decay on either side from the center of each peak. The periodic structure in a lump wave configuration arises out of nonlinear interactions in the system that make it possible to obtain a stable repetitive configuration. Contour plot display in Figure 8(b) displays the time stable states of the multisolitons. Clearly defined peaks in them attest their coherent propagation. The 2D plot in Figure 8(c) present the formation and movement of multi-soliton waves. The $t = 0$ (red), $t = 1$ (blue), and $t = 2$ (green) profiles are distinct and stable, characteristic of the solitonic interaction. The 3D representation of a periodic cross-kink wave is shown in Figure 9(a). It captures repetitive periodicities of cross-kinks. Periodic overlap of structures indicates possible nonlinear interaction effects of wave propagation by kink-like waves propagating at different orientations. The contour plot of Figure 9(b) captures the cross-pattern of periodic distribution of the kinks, indicating stable propagation and periodic overlaps of the kink structures. The 2D plot of Figure 9(c) demonstrate the stability of cross-kinks. The coherent dynamics and robust structure of the periodic waveforms are shown at $t = 0$ (red), $t = 1$ (blue), and $t = 2$ (green). The 3D representation of a periodic cross-kink wave is shown in Figure 10(a). It flexes the traveling solitons periodically with a train structure. These solitons maintain their amplitude and phase during propagation uniformly in the medium. It reflects soliton stability and periodicity in the wave system. The contour plot of Figure 10(b) captures its periodic nature with equally spaced and uniform stripes of solitons. Such patterns show the coherent propagation of solitons without any amplitude decay and with minimal interaction. The 2D plot of Figure 10(c) with varying time at $t = 0$ (red), $t = 1$ (blue), and $t = 2$ (green) shows the solitons keeping their amplitude and the wavelength remain the same with shape over time, thus proving its solitary nature and stable periodic soliton trains supported by the medium. The 3D surface plot delineated in Figure 11(a) is derived from a homoclinic breather wave structure; it depicts the breather solution, with oscillatory growth and decay localized within certain regions. While in Figure 11(b), the contour plot highlights periodic localizing and delocalizing of the wave energy, which is a feature of breather solutions observed in nonlinear systems. In Figure 11(c), the 2D graph shows $t = 0$ (red), $t = 1$ (blue), and $t = 2$ (green), where there is an oscillatory amplitude increase and decrease, conferring to the period energy trapping and releasing of the breather. In Figure 12(a), it is evident from the 3D plot, which indicates a unique energy concentration in the center and has oscillations decayed symmetrically toward the boundaries, which this localized oscillatory form is indicative of the localized oscillatory nature of homoclinic breathers. The contour plot in Figure 12(b) emphasizes the central localization of energy, with oscillatory patterns tapering off in the surrounding areas, also supports the interpretation homoclinic breather in this regard. The 2D plot in Figure 12(c) show plots at $t = 0$ (red) and $t = 1$ (blue) representing the wave amplitude. They demonstrate localized oscillations, which grow and decay symmetrically; it indicates homoclinic breather dynamics. The amplitude decreases as the oscillations move outward, a characteristic feature of homoclinic structures.

These analysis provides overall insight into the rich dynamical behaviors displayed by the exact solutions of the (3+1)-dimensional CIE. Figure 1 shows shape and amplitude preserving bright solitons in propagation, indicating stability. Figure 2 shows localized dips (dark solitons) that move without distortion, which suggests elastic interactions. Figure 3 shows an M-shaped wave with a single kink that displays a sudden amplitude transition along with symmetric wave motion. In Figure 4, the interaction of an M-shaped wave with a rogue structure and a kink displays intense nonlinear effects such as the sudden amplification of energy. Figure 5 depicts mixed waves created by several functional components, resulting in interference complexity and oscillatory modulation. Figure 6 shows oscillatory solitons with periodic modulation of the amplitude, supported by nonlinear dispersion balance. Figure 7 presents multi wave structures with breather-like behavior, wherein periodic exchange of energy takes place between wave modes. Figure 8 illustrates periodic lump waves with sharp, localized crests and periodic intervals, indicating strong spatial confinement. Figure 9 illustrates periodic cross-kinks resulting from the intersection of kink structures, exhibiting multidimensionality propagation. Figure 10 shows periodic kink trains that travel uniformly, which is characteristic of repeated nonlinear transitions with phase coherence. Figure 11 displays homoclinic breathers with space- and time-localized symmetric oscillations, indicative of temporary energy trapping. Finally, Figure 12 highlights a sharper and more localized homoclinic breather with intense central localization and controlled decay of oscillations. Collectively, these confirm the analytical results and illustrate the wealth of nonlinear wave dynamics described by the Hirota bilinear technique in a multidimensional context.

Figure 1(a) illustrates the 3D plot of solution $N_{1IE}(x, y, z, t)$ for Eq. (12) for choosing parameters $L_2 = 0.2$, $L_4 = 12.5$, $P_1 = 8.7$, $P_2 = 15.3$, $a = 6.8$, $b = 0.3$, $c = 0.7$, $d = 6.1$, $h = 0.7$, $y = 1.8$, $z = 11.2$. Figure 1(b)

provides the contour diagram, and Figure 1(c) presents its 2D plot.

Figure 2(a) illustrates the 3D plot of solution $N_{2IE}(x, y, z, t)$ for Eq. (13) for choosing parameters $L_2 = 1.9$, $L_4 = 1.2$, $P_1 = 1.1$, $P_2 = 7.4$, $a = 3.1$, $b = 0.09$, $c = 1.1, d = 1.1, h = 3.7, y = 6.4, z = 2.7$. Figure 2(b) provides the contour diagram, and Figure 2(c) presents its 2D plot.

Solution $N_{1M1K}(x, y, z, t)$ associated with Eq. (15) is portrayed as a 3D in Figure 3(a) by the choice of parameter values $L_2 = 14.7$, $L_4 = 2.2$, $L_6 = 2.1$, $L_7 = 10.1$, $P_1 = 3.6$, $a = 8.8$, $b = 0.1$, $c = 4.3$, $d = 2.4$, $y = 1.7$, $z = 3.7$. Figure 3(b) and (c) demonstrate, respectively, its contour and 2D plots.

The 3D plot for solution ($N_{1MRK}(x, y, z, t)$) of Eq. (17) at the chosen parameter values of $L_2 = 0.35, L_4 = 1.3, P_1 = 2.6, P_2 = 0.9, P_4 = 9.9, a = 1.6, b = 2.0, c = 0.2, d = 0.1, y = 1.0, z = 5.5$ is shown in Figure 4(a). Figure 4(b) and (c) provide its contour and 2D plots, respectively.

The 3D in Figure 5(a) is depicted from the solution $N_{1MI}(x, y, z, t)$ corresponding to Eq. (19) for chosen parameter values $L_2 = 2.3, L_4 = 13.3, L_6 = 4.1, P_1 = 2.7, P_2 = 1.6, P_3 = 2.7, P_4 = 1.6, a = 10.7, b = 0.8, c = 2.5, d = 1.2, h = 1.9, y = 1.6, z = 18.2$. Figure 5(b) and (c) show the corresponding contour and 2D plots.

The 3D in Figure 6(a) is depicted from the solution $N_{2MI}(x, y, z, t)$ corresponding to Eq. (20) for chosen parameter values $L_2 = 5.6, L_4 = 12.6, L_6 = 9.3, P_1 = 3.6, P_3 = 4.1, P_4 = 1.7, a = 1.3, b = 0.5, c = 1.8, d = 6.5, h = 0.5, y = 5.1, z = 2.3$. Figures 6(b) and (c) show the corresponding contour and 2D plots, respectively.

The 3D plot in Figure 7(a), corresponding to Eq. (22), generated from solution $N_{1MU}(x, y, z, t)$ for the parameter values $L_2 = 0.09$, $L_4 = 8.9$, $P_1 = 2.8$, $P_2 = 17.3$, $a = 1.9$, $b = 15.9$, $c = 14.8$, $d = 10.2$, $y = 11.2$, $z = 15.8$. Figure 7(b) provides the contour, while Figure 7(c) shows the 2D plot.

Figure 8(a) illustrates the 3D plot of solution $N_{1PL}(x, y, z, t)$ for Eq. (24) for choosing parameters $L_6 = 2.5$, $a = 0.8$, $b = 16.7$, $c = 1.5$, $d = 1.05$, $y = 10.3$, $z = 3.5$. Figure 8(b) provides the contour diagram, and Figure 8(c) presents its 2D plot.

The 3D graph of solution $N_{1PCK}(x, y, z, t)$, corresponding to Eq. (26), Figure 9(a) is obtained by selecting parameter values $L_2 = 10.7$, $L_4 = 5.3$, $L_6 = 14.5$, $L_8 = 11.2$, $P_1 = 9.5$, $P_2 = 12.3$, $P_3 = 7.8$, $a = 7.1$, $b = 1.2$, $c = 8.7$, $d = 1.7$, $h = 8.6$, $y = 2.3$, $z = 4.5$. Figure 9(b) and (c) shows the contours and 2D images, respectively.

The 3D graph of solution $N_{2PCK}(x, y, z, t)$, corresponding to Eq. (27), Figure 10(a) is obtained by selecting parameter values $L_2 = 5.4$, $L_6 = 2.8$, $L_8 = 4.3$, $P_2 = 12.3$, $P_3 = 3.2$, $a = 2.2$, $b = 0.6$, $c = 8.7$. $d = 1.7$, $h = 0.1$, $y = 10.3$, $z = 12.2$. Figure 10(b) and (c) shows the contours and 2D images, respectively.

The 3D visualization of solution $N_{1HB}(x, y, z, t)$, corresponding to Eq. (28), Figure 11(a) is obtained by selecting parameter values $L_2 = 15.3$, $L_4 = 15.0$, $L_5 = 7.7$, $L_6 = 10.8$, $P_1 = 0.6$, $P_2 = 0.8$, $P_3 = 1.8$, $a = 18.8$, $b = 0.1$, $c = 16.8$, $d = 18.0$, $y = 18.9$, $z = 1.7$. The corresponding contour and 2D graphs are shown in Figure 11(b) and (c), respectively.

The 3D visualization of solution $N_{2HB}(x, y, z, t)$, corresponding to Eq. (28), Figure 12(a) is obtained by selecting parameter values $L_4 = 2.4$, $L_5 = 3.6$, $L_6 = 1.8$, $P_2 = 3.8$, $P_3 = 9.7, a = 6.8, b = 0.1, c = 2.8, d = 18.7, y = 16.2, z = 17.1$. The corresponding contour and 2D graphs are shown in Figures 12(b) and (c), respectively.

4 Result comparison

The solutions thus derived in this research with the Hirota bilinear method clearly differ from the solutions produced by other popular analytical methods that were previously used on the CIE. This research systematically derives a wide range of exact solutions in (3+1) dimensions of the CIE such as bright and dark solitons, M-shaped waves, periodic cross-kinks, rogue-kink interactions, lump waves, breathers, and multiwave forms with rich spatial-temporal dynamics. Contrarily, the GERF method, first integral method, and expansion methods have been used mostly to the (1+1) and (2+1)-dimensional forms of the equation. These techniques generally obtain bright solitons, dark solitons, kink and anti-kink solutions, and singular and periodic waveforms [24–26]. For instance, the GERF and expansion methods have generated combined soliton and oscillatory patterns [25,29], whereas the first integral method has been able to generate solitary waves and periodic patterns in a more limited dimensional framework [26]. Also, Khater and Alfalq [30] investigated the fractional nonlinear generalized (3+1)-dimensional CIE to model wave propagation in dispersive media *via* the Khat II and He's variational iteration approaches, obtaining both analytical and numerical solutions. These studies, despite being indicative of the multifunctional nature of the equation, are more directed toward system simulation and stability rather than the synthesis of wide families of diverse interacting solutions.

While approaches like modified F-expansion [19], modified Khater method [22], MAE method [27], and stochastic formulations [14,18] have given useful results in examining the dynamics of a system, these lack the complete understanding of intricate multisoliton interactions as well as the combination wave formations possible with natural revelation using Hirota's bilinear method. In addition,

the Hirota scheme has already been used effectively in more recent studies of higher-dimensional nonlinear systems, further solidifying its image as a versatile and robust scheme for the study of complex wave symmetries. Thus, the present research not only extends the class of previously known solutions to the (3+1)-dimensional CIE but also enhances our knowledge of nonlinear wave dynamics by symbolic derivation and visual interpretation, going beyond the capabilities of most of the methods employed earlier.

5 Conclusion

The Hirota bilinear transform method has shown to be an effective technique to investigate different types of wave symmetries of the (3+1)-dimensional CIE. It has worked well in this study using the power of the Mathematica program by deriving and graphing a number of exact solutions such as bright and dark solitons, periodic cross kinks, breathers, multi waves, mixed waves, and lump waves, among others, which form part of a very important class of solutions, each having its own dynamic properties yet retained in symmetry to the original equation. Indeed, such solutions made one appreciate the really fine balance that exists between nonlinearity and dispersion for stable wave propagation in high-dimensional nonlinear media. Such solutions were also analyzed graphically to obtain better insights as regarding their spatial and temporal behaviors, while under various conditions, the latter expounding on their stability and coherence.

These phenomena and other effects are properties of the equation in modeling complex and highly nonlinear interactions, such as the elastic collisions of solitary waves or periodic overlaps of kinks. Breather and homoclinic breather solutions produce localized oscillatory states that encode information concerning the energetic modulation and phase evolution. With these features, it is possible to note the capacity of the (3+1)-dimensional CIE to cater some rich and multidimensional wave behavior and make it an excellent model for theoretical and practical studies.

The originality of the present work is in the use of the Hirota bilinear formalism to the (3+1)-dimensional CIE, an area that has not received much attention in the literature. Through the production of a rich diversity of exact wave patterns from M-shaped waves, lump, and breathers to mixed interactions, this research contributes to the analytical knowledge of multidimensional soliton dynamics. The importance of these results lies in their potential to simulate real nonlinear processes in physical systems in which dimensional complexity is of decisive importance. Not only do these results extend the range of applications of soliton theory, but they also represent a useful starting point for future research in applied mathematics and physics.

It is worth noting that all the solutions obtained have been verified and found to satisfy the governing equation. Finally, this contribution will further our understanding of nonlinear wave dynamics by opening up new avenues for discovering and enlarging wave symmetries in the (3+1)-dimensional CIE. The results demonstrate the power of the Hirota bilinear transformations method in awakening coherently and stably wave structures within various nonlinear regimes. Moving with this solid analytical backbone, the work encourages further research on high-dimensional systems and expands the scope of the nonlinear wave theory, catering to basic and applied science.

Future work can focused on extending the Hirota bilinear transformation approach to fractional and variable-coefficient forms of the (3 + 1) dimensional CIE, and other higher-order NLPDEs. In addition, incorporating perturbation effects, external potentials, or numerical simulations can be employed to validate and generalize the analytical findings, leading to better understanding into real-world applications such as nonlinear optics, fluid dynamics, and signal transmission in complex media.

Funding information: The authors state no funding involved.

Author contributions: Conceptualization, N.A. and J.E.M.-D.; methodology, N.A. and J.E.M.-D.; software, B.C., M.Z.B., N.A., N.S., S.M., and J.E.M.-D.; validation, B.C., M.Z.B., N.A., N.S., S.M., and J.E.M.-D.; formal analysis, B.C., M.Z.B., N.A., N.S., S.M., and J.E.M.-D.; investigation, B.C., M.Z.B., N.A., N.S., S.M., and J.E.M.-D.; resources, B.C., M.Z.B., N.A., N.S., S.M., and J.E.M.-D.; data curation, M.Z.B., N.S., and S.M.; writing-original draft, B.C., M.Z.B., N.A., N.S., S.M., and J.E.M.-D.; writing-review and editing, B.C., M.Z.B., N.A., N.S., S.M., and J.E.M.-D.; visualization, B.C., M.Z.B., and N.S.; supervision N.A. and J.E.M.-D. All authors have read and agreed to the published version of the manuscript. B.C., M.Z.B., N.A., N.S., S.M., and J.E.M.-D. All authors have accepted responsibility for the entire content of this manuscript and approved its submission.

Conflict of interest: The authors state no conflict of interest.

Data availability statement: Data sharing is not applicable to this article as no new data were created or analyzed in this study.

References

[1] Mohan B, Kumar S. Generalization and analytic exploration of soliton solutions for nonlinear evolution equations via a novel symbolic approach in fluids and nonlinear sciences. Chin J Phys. 2024;92:10–21.

[2] Kumar S, Mohan B, Kumar R. Lump, soliton, and interaction solutions to a generalized two-mode higher-order nonlinear evolution equation in plasma physics. Nonlinear Dyn. 2022;110(1):693–704.

[3] AlQahtani SA, Alngar ME, Shohib RM, Alawwad AM. Enhancing the performance and efficiency of optical communications through soliton solutions in birefringent fibers. J Optics. 2024;53:1–11.

[4] Shohaib M, Masood W, Shah HA, Almuqrin AH, Ismaeel SM, El-Tantawy SA. On the dynamics of soliton interactions in the stellar environments. Phys Fluids. 2024;36(2):025164.

[5] Dauda UM, Musa SS, Iyanda FK. Dynamics of DNA: nonlinear interaction of solitons. 2024. Available at SSRN 4929897.

[6] Shakeel M, Liu X, Mostafa AM, AlQahtani NF, Alameri A. Dynamic solitary wave solutions arising in nonlinear chains of atoms model. J Nonl Math Phys. 2024;31(1):70.

[7] Shakeel M, Abbas N, Rehman MJU, Alshammari FS, Al-Yaari A. Lie symmetry analysis and solitary wave solution of biofilm model Allen-Cahn. Sci Rep. 2024;14(1):12844.

[8] Abbas N, Shakeel M, Fouly A, Ahmadian H. Numerical simulations and analytical approach for three-component coupled NLS-type equations in fiber optics. Modern Phys Let B, 2025;39(2):2450390.

[9] Sahoo AK, Gupta AK, Seadawy AR On the solutions of space-time fractional CBS and CBS-BK equations describing the dynamics of Riemann wave interaction. Int J Modern Phys B. 2025;39(04):2540001.

[10] Seadawy AR, Alsaedi BA. Variational principle for generalized unstable and modify unstable nonlinear Schrödinger dynamical equations and their optical soliton solutions. Opt Quantum Electron. 2024;56(5):844.

[11] Constantin P, Foias C, Nicolaenko B, Temam R. Integral manifolds and inertial manifolds for dissipative partial differential equations. Vol. 70. New York: Springer Science Business Media; 2012.

[12] Hossain MM, Akter S, Roshid MM, Sheikh MAN. Dynamical property of interaction solutions to the Chafee–Infante equation via NMSE method. Heliyon. 2024;10(16):e36168.

[13] Caraballo T, Langa JA, Robinson JC. Stability and random attractors for a reaction–diffusion equation with multiplicative noise. Discrete Contin Dyn Syst. 2000;6(4):875–92.

[14] Caraballo T, Crauel H, Langa J, Robinson J. The effect of noise on the Chafee–Infante equation: a nonlinear case study. Proc Am Math Soc. 2007;135(2):373–82.

[15] Debussche A, Högele M, Imkeller P. Asymptotic first exit times of the Chafee–Infante equation with small heavy-tailed Lévy noise. Berlin: Springer;2011.

[16] Rosa R. Exact finite dimensional feedback control via inertial manifold theory with application to the Chafee–Infante equation. J Dyn Differ Equ. 2003;15(1):61–86.

[17] Carvalho A, Langa J, Robinson J. Structure and bifurcation of pullback attractors in a non-autonomous Chafee–Infante equation. Proc Am Math Soc. 2012;140(7):2357–73.

[18] Blumenthal A, Engel M, Neamtu A. On the pitchfork bifurcation for the Chafee–Infante equation with additive noise. Probability Theory Related Fields. 2023;187(3):603–27.

[19] Tang X, Wang Y. Soliton dynamics for generalized Chafee–Infante equation with power-law nonlinearity. Europ Phys J D. 2023;77(10):179.

[20] Hossain MM, Akter S, Roshid MM, Sheikh MAN. Dynamical property of interaction solutions to the Chafee–Infante equation via NMSE method. Heliyon. 2024;10(16):e36168.

[21] Rached Z. On exact solutions of Chafee–Infante differential equation using enhanced modified simple equation method. J Interdiscipl Math. 2019;22(6):969–74.

[22] Mahmood A, Abbas M, Akram G, Sadaf M, Riaz MB, Abdeljawad T. Solitary wave solution of (2+1)-dimensional Chaffee-Infante equation using the modified Khater method. Results Phys. 2023;48:106416.

[23] Arshed S, Akram G, Sadaf M, Irfan M, Inc M. Extraction of exact soliton solutions of (2+1)-dimensional Chaffee-Infante equation using two exact integration techniques. Opt Quantum Electron. 2024;56(6):1–15.

[24] Arshed S, Akram G, Sadaf M, Bilal Riaz M, Wojciechowski A. Solitary wave behavior of (2+1)-dimensional Chaffee-Infante equation. Plos One. 2023;18(1):e0276961.

[25] Kumar S, Almusawa H, Hamid I, Akbar MA, Abdou MA. Abundant analytical soliton solutions and evolutionary behaviors of various wave profiles to the Chaffee-Infante equation with gas diffusion in a homogeneous medium. Results Phys. 2021;30:104866.

[26] Akbar MA, Ali NHM, Hussain J. Optical soliton solutions to the (2+1)-dimensional Chaffee-Infante equation and the dimensionless form of the Zakharov equation. Adv Differ Equ. 2019;2019(1):446.

[27] Cimpoiasu R. Multiple explicit solutions of the 2D variable coefficients Chafee–Infante model via a generalized expansion method. Modern Phys Let B. 2021;35(19):2150312.

[28] Khater M, Ghanbari B. On the solitary wave solutions and physical characterization of gas diffusion in a homogeneous medium via some efficient techniques. Europ Phys J Plus. 2021;136(4):1–28.

[29] Sebogodi MC, Muatjetjeja B, Adem AR. Traveling wave solutions and conservation laws of a generalized Chaffee-Infante equation in (1+3) dimensions. Universe. 2023;9(5):224.

[30] Khater MM, Alfalqi SH. Dissipation and dispersion in fractional nonlinear wave dynamics: Analytical and numerical explorations. Fractals. 2024;32(07–08):1–19.

[31] Yin T, Xing Z, Pang J. Modified Hirota bilinear method to (3+1)-D variable coefficients generalized shallow water wave equation. Nonlinear Dyn. 2023;111(11):9741–52.

[32] Li Y, Yao R, Lou S. An extended Hirota bilinear method and new wave structures of (2+1)-dimensional Sawada-Kotera equation. Appl Math Lett. 2023;145:108760.

[33] Yokus A, Isah MA. Dynamical behaviors of different wave structures to the Korteweg-de Vries equation with the Hirota bilinear technique. Phys A Stat Mech Appl. 2023;622:128819.

[34] Zhang J, Manafian J, Raut S, Roy S, Mahmoud KH, Alsubaie ASA. Study of two soliton and shock wave structures by weighted residual method and Hirota bilinear approach. Nonlinear Dyn. 2024;112:1–17.

[35] Ceesay B, Ahmed N, Macías-Díaz JE. Construction of M-shaped solitons for a modified regularized long-wave equation via Hirotaas bilinear method. Open Phys. 2024;22(1):20240057.

[36] Kumar S, Mohan B. A novel and efficient method for obtaining Hirotaas bilinear form for the nonlinear evolution equation parque Pikillactain (n+1) dimensions. Partial Differ Equ Appl Math. 2022;5:100274.

[37] Ahmad S, Saifullah S, Khan A, Inc M. New local and nonlocal soliton solutions of a nonlocal reverse space-time mKdV equation using improved Hirota bilinear method. Phys Lett A. 2022;450:128393.
[38] Gu Y, Peng L, Huang Z, Lai Y. Soliton, breather, lump, interaction solutions and chaotic behavior for the (2+1)-dimensional KPSKR equation. Chaos Solitons Fractals. 2024;187:115351.
[39] Gu Y, Zhang X, Huang Z, Peng L, Lai Y, Aminakbari N. Soliton and lump and travelling wave solutions of the (3+1)-dimensional KPB like equation with analysis of chaotic behaviors. Scientif Reports. 2024;14(1):20966.
[40] Shehzad F, Zahed H, Rizvi ST, Ahmed S, Abdel-Khalek S, Seadawy AR. Generalized breather, solitons, rogue waves, and lumps for superconductivity and drift cyclotron waves in plasma. Brazilian J Phys. 2025;55(3):118.
[41] Ceesay B, Baber MZ, Ahmed N, Akgül A, Cordero A, Torregrosa JR. Modelling symmetric ion-acoustic wave structures for the BBMPB equation in fluid ions using Hirota's bilinear technique. Symmetry. 2023;15(9):1682.
[42] Ozsahin DU, Ceesay B, Baber MZ, Ahmed N, Raza A, Rafiq M, et al. Multiwaves, breathers, lump and other solutions for the Heimburg model in biomembranes and nerves. Sci Rep. 2024;14(1):10180.
[43] Ceesay B, Ahmed N, Baber MZ, Akgül A. Breather, lump, M-shape and other interaction for the Poisson-Nernst-Planck equation in biological membranes. Opt Quantum Electron. 2024;56(5):853.
[44] Ceesay B, Baber MZ, Ahmed N, Yasin MW, Mohammed WW. Breather, lump and other wave profiles for the nonlinear Rosenau equation arising in physical systems. Scientif Reports. 2025;15(1):3067.